GEOPHYSICS, VOL. 78, NO. 4 (JULY-AUGUST 2013); P. A29–A33, 4 FIGS.
10.1190/GEO2013-0044.1

Time-lapse image-domain tomography using adjoint-state methods

Jeffrey Shragge[1], Tongning Yang[2], and Paul Sava[2]

ABSTRACT

Adjoint-state methods (ASMs) have proven successful for calculating the gradients of the functionals commonly found in geophysical inverse problems. The 3D ASM image-domain tomography (IDT) formulation of the seismic velocity estimation problem highlights imperfections in migrated image volumes and, using appropriate penalty functions (e.g., differential semblance), forms an objective function that can be minimized using standard optimization approaches. For time-lapse (4D) seismic scenarios, we show that the 3D ASM-IDT approach can be extended to multiple (e.g., baseline and monitor) data sets and offers high-quality estimates of subsurface velocity change. We discuss two different penalty operators that lead to absolute and relative 4D inversion strategies. The absolute approach uses the difference of two independent 3D inversions to estimate a 4D model perturbation (i.e., slowness squared). The relative approach inverts for the model perturbation that optimally matches the monitor image to the baseline image — even if migrated energy is imperfectly focused. Both approaches yield good 4D slowness estimates; however, we assert that the relative approach is more robust given the ubiquitous presence of nonrepeatable 4D acquisition noise and imperfect baseline model estimates.

INTRODUCTION

Adjoint-state methods (ASMs) have been used with success for many years in seismic exploration as an effective approach for calculating the gradient of a functional (see the overviews of Plessix, 2006 and Symes, 2008). Whereas most of studies focus on data-domain implementations — in particular, full waveform inversion (FWI) (Tarantola, 1984; Pratt, 1999) — several studies explore complementary image-domain tomography (IDT) strategies (Albertin et al., 2006; Yang and Sava, 2011). Rather than posing an objective function based on differences between modeled and field data, the more kinematically biased IDT inversion approaches use objective functions that measure observed imperfections in migrated images (i.e., poorly focused extended image gathers [EIGs]). Similar to data-domain FWI approaches, these imperfections are back projected using ASM machinery to form gradient estimates appropriate for velocity model updating.

Because image-domain approaches do not match data amplitudes and thereby wavefield dynamics, they afford lower resolution than data-domain methods; however, they are less sensitive to the manifold factors affecting seismic amplitudes (e.g., attenuation, irregular illumination). Although normally considered a negative trait, one corollary is that ASM-IDT inversions are more robust than data-domain ASM approaches because they satisfy less-demanding inversion criteria. This leads to an increased likelihood of converging toward correct, though necessarily more band-limited, inversion results. Model perturbations derived from ASM-IDT analyses are thus useful when used either outright as a final 3D migration velocity model or as the input to higher resolution data-domain FWI analysis.

The 3D ASM-IDT goal is to invert for the model slowness perturbation $\Delta s_1 \equiv s_1 - s_0$ that optimally focuses the image and (supposedly) represents the difference between the true and assumed background models s_1 and s_0, respectively. A key decision in the ASM-IDT inversion procedure is to specify a judicious penalty operator that (1) eliminates energy already optimally focused in the extended image gather volume at the zero correlation lag and (2) upweights energy that is poorly focused at nonzero correlation lags. A common way to accomplish this is through applying a differential semblance operator (DSO) (Symes and Carazzone, 1991; Shen et al., 2005), which cancels out a perfectly focused image at zero correlation lag. However, there are other classes of penalty functions that can be used in the ASM-IDT inversion procedure; e.g., ones that compensate for illumination irregularities (Yang et al., 2012) or more fully account for scattering theory (Albertin, 2011).

Manuscript received by the Editor 7 February 2013; revised manuscript received 2 April 2013; published online 20 June 2013.
[1]The University of Western Australia, School of Earth and Environment, Centre for Petroleum Geoscience and CO_2 Sequestration, Crawley, Australia. E-mail: jshragge@gmail.com.
[2]Colorado School of Mines, Department of Geophysics, Center for Wave Phenomena, Golden, Colorado, USA. E-mail: tyang@mines.edu; psava@mines.edu.

The 4D ASM-IDT velocity estimation problem shares many similarities with, and may be regarded an extension of, 3D ASM-IDT inversion. Two key differences are that there are now multiple data sets to work with as well as multiple slowness perturbations to recover (i.e., baseline Δs_1, monitor Δs_2, and the time-lapse Δs_{TL} differences). Unlike the 3D problem where one seeks the *absolute* slowness perturbation that optimally focuses reflectivity at zero correlation lag, for 4D applications, one can use either an *absolute* or a *relative* inversion strategy when estimating Δs_{TL}. The former is achieved by setting up two separate tomographic inversions that independently estimate Δs_1 and Δs_2 and then taking their difference. Alternatively, one may estimate a relative 4D slowness difference by coupling the baseline and monitor data sets in the inversion procedure and finding the slowness perturbation that optimally matches the monitor image to the baseline image.

Herein, we examine the utility of 4D ASM-IDT methods by exploring a new class of 4D penalty functions generated from the baseline image volume that are multiplicatively applied to the monitor data set when inverting for a relative Δs_{TL} estimate. The 4D penalty operator minimizes energy colocated in the baseline and monitor image volumes, even where not optimally focused, while upweighting energy inconsistent between the two images. We begin by briefly reviewing 3D ASM-IDT theory and discussing the absolute and relative 4D ASM-IDT extensions. We then present the results of 4D absolute and relative 4D ASM-IDT inversion experiments that highlight the advantages of using a relative strategy.

3D ASM-IDT THEORY

Given a one-way acoustic frequency-domain wave operator $\mathcal{L} = \mathcal{L}(\mathbf{x}, \omega, m_1)$ and its adjoint, $\mathcal{L}^\dagger$, we write the 3D forward modeling problem as

$$\begin{bmatrix} \mathcal{L} & 0 \\ 0 & \mathcal{L}^\dagger \end{bmatrix} \begin{bmatrix} u_s(\mathbf{e_1}, \mathbf{x}, \omega) \\ u_r(\mathbf{e_1}, \mathbf{x}, \omega) \end{bmatrix} = \begin{bmatrix} f_s(\mathbf{e_1}, \mathbf{x}, \omega) \\ f_r(\mathbf{e_1}, \mathbf{x}, \omega) \end{bmatrix}, \tag{1}$$

where m_1 are the model parameters (i.e., square of the slowness field, $m_1 = s_1^2$); $\mathbf{x}$ are the spatial coordinates; ω is the frequency; u_s and u_r are the computed source and receiver wavefields for source index $\mathbf{e_1}$; and f_s and f_r are the source and recorded data. The derivative of modeling operator $\mathcal{L} = -\omega^2 m_1 - \nabla^2$ with respect to model parameters m_1 is $\partial\mathcal{L}/\partial m_1 = -\omega^2$. State variables u_s and u_r, both solutions to the acoustic wave equation, are used to formulate an objective function, $\mathcal{H}$ that, for the ASM-IDT problem, is based on minimizing image imperfections (i.e., a poorly focused extended image volume) caused by an unknown model perturbation Δm_1,

$$\mathcal{H} = \frac{1}{2} \| P_1(\mathbf{x}, \boldsymbol{\lambda}) r_1(\mathbf{x}, \boldsymbol{\lambda}) \|^2_{\mathbf{x},\boldsymbol{\lambda}}. \tag{2}$$

The EIG volume $r_1(\mathbf{x}, \boldsymbol{\lambda})$ is formed by crosscorrelating the state variables in the direction denoted by $\boldsymbol{\lambda}$ (herein horizontal),

$$r_1(\mathbf{x}, \boldsymbol{\lambda}) = \sum_{\mathbf{e_1},\omega} \overline{u_s(\mathbf{e_1}, \mathbf{x} - \boldsymbol{\lambda}, \omega)}\, u_r(\mathbf{e_1}, \mathbf{x} + \boldsymbol{\lambda}, \omega). \tag{3}$$

Penalty operator $P_1(\mathbf{x}, \boldsymbol{\lambda})$ highlights the defocusing in $[\mathbf{x}, \boldsymbol{\lambda}]$ hypercube within extended image $r_1(\mathbf{x}, \boldsymbol{\lambda})$. In the absence of other information, one can use the DSO penalty function $P_1(\mathbf{x}, \boldsymbol{\lambda}) = P_\lambda(\boldsymbol{\lambda}) = |\boldsymbol{\lambda}|$ (Figure 1a) shown elsewhere to produce high-quality inversion results (Symes and Carazzone, 1991; Shen et al., 2005).

Having defined a penalty function the adjoint sources and receiver g_s and g_r are formed by taking the derivatives of $\mathcal{H}$ (equation 2) with respect to state variables $\overline{u_s}$ and $\overline{u_r}$:

$$\begin{bmatrix} g_s(\mathbf{e_1}, \mathbf{x}, \omega) \\ g_r(\mathbf{e_1}, \mathbf{x}, \omega) \end{bmatrix} = \begin{bmatrix} \sum_{\boldsymbol{\lambda}} P_1^2(\mathbf{x}, \boldsymbol{\lambda}) \overline{r_1(\mathbf{x}, \boldsymbol{\lambda})} u_r(\mathbf{e_1}, \mathbf{x} + \boldsymbol{\lambda}, \omega) \\ \sum_{\boldsymbol{\lambda}} P_1^2(\mathbf{x}, \boldsymbol{\lambda}) r_1(\mathbf{x}, \boldsymbol{\lambda}) u_s(\mathbf{e_1}, \mathbf{x} - \boldsymbol{\lambda}, \omega) \end{bmatrix}. \tag{4}$$

Adjoint-state variables a_s and a_r are the wavefields obtained by adjoint and forward modeling of the corresponding adjoint sources and receivers analogous to equation 1:

$$\begin{bmatrix} \mathcal{L}^\dagger & 0 \\ 0 & \mathcal{L} \end{bmatrix} \begin{bmatrix} a_s(\mathbf{e_1}, \mathbf{x}, \omega) \\ a_r(\mathbf{e_1}, \mathbf{x}, \omega) \end{bmatrix} = \begin{bmatrix} g_s(\mathbf{e_1}, \mathbf{x}, \omega) \\ g_r(\mathbf{e_1}, \mathbf{x}, \omega) \end{bmatrix}. \tag{5}$$

The gradient estimate is then formed by correlating the state and adjoint-state variables:

$$\frac{\partial \mathcal{H}}{\partial m_1} = -\sum_{\mathbf{e_1},\omega} \omega^2 (\overline{u_s} a_s + u_r \overline{a_r}). \tag{6}$$

Finally, the model parameter update Δm_1 is found through an iterative nonlinear gradient-based method (Knyazev and Lashuk, 2007) where, at each iteration, the computed gradient is used in a parabolic line search based on the steepest descent (iteration 1) or conjugate gradient directions (successive iterations). The iterative process continues until, ideally, one meets the convergence criterion and recovers the optimal slowness perturbation estimate.

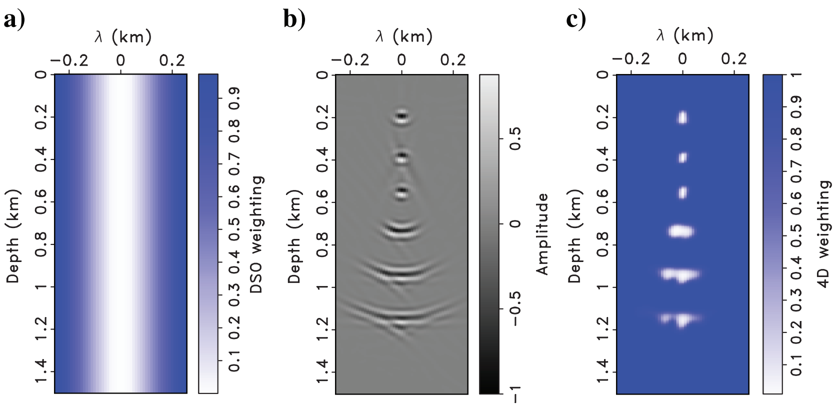

Figure 1. (a) Penalty function $P_\lambda = |\boldsymbol{\lambda}|$. (b) Sample EIG from baseline image r_1. (c) Penalty function $P_{4D} = P_{4D}(r_1)$.

4D ASM-IDT THEORY

As discussed above, there are two different strategies to the time-lapse ASM-IDT inversion problem: *absolute* and *relative*. In the absolute approach, one performs separate 3D ASM-IDT inversions to obtain independent estimates of the baseline and monitor slowness perturbations from a common slowness model (i.e., Δs_1 and Δs_2). The time-lapse estimate is assumed to be their difference $\Delta s_{\mathrm{TL}} \equiv \Delta s_2 - \Delta s_1$. Specifying the monitor ASM-IDT inversion problem requires only replacing subscript 1 with 2 in equations 1–6 above (e.g., replace $\mathbf{e_1}$ with $\mathbf{e_2}$) and then calculating the monitor-baseline estimate difference. Judicious 4D practice would suggest that one should use the same penalty operator $P_1 = P_2 = P_\lambda$ in the two independent inversions; to do otherwise would lead to inconsistently weighted back projections and cause an erroneous Δs_{TL} estimate.

The relative 4D approach recognizes that there is prior information in the baseline image that one can incorporate into the penalty function used in the monitor inversion. That is, we may use a penalty function $P_2 = P_{4D}(r_1)$ designed to remove the imaged reflectivity that is consistent between the baseline and monitor images, leaving only monitor image energy that does not match. Applying P_{4D} in place of P_λ in equations 2 and 4 to the monitor data set will emphasize different residual energy and lead to different monitor inversion results.

Figure 1c presents a 4D penalty derived from image r_1 in Figure 1b defined by $P_{4D} = \mathrm{sech}^2\left(\langle r_1^2\rangle / \max(\langle r_1^2\rangle)\right)$. Symbol $\langle\cdot\rangle$ indicates that we conditioned r_1^2 by taking a (symmetric, five-point, triangularly) smoothed image envelope after applying a 3D AGC operator to upweight weaker reflector amplitudes toward those of the stronger ones. Although most energy is focused about $\boldsymbol{\lambda} = 0$, some residual exists at nonzero lags indicating an imperfect migration slowness model. Applying this weighting function largely cancels out energy common to both images, even where it is equally poorly focused. Accordingly, the only contributions to the 4D estimate (ideally) will be from the *relative* baseline-monitor image changes and not those from an inaccurate/incomplete baseline analysis. Importantly for 4D practice, this approach does not rely on baseline-monitor data/image differences, which are notoriously noisy due to nonrepeatable 4D acquisition and therefore more likely to lead to erroneous 4D velocity inversion results.

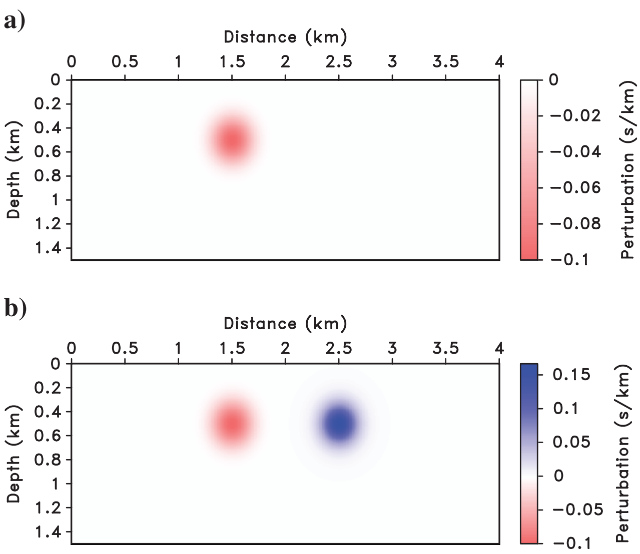

Figure 2. Slowness perturbations from a constant $s_0 = 0.5$ s/km model. (a) Baseline Δs_1. (b) Baseline plus monitor $\Delta s_1 + \Delta s_2$.

EXPERIMENT

Our numerical experiments test the validity of the two time-lapse inversion approaches in a relatively noise-free environment. Figure 2a presents the baseline slowness perturbation Δs_1 from a constant P-wave ($s_0 = 0.5$ s/km) background, whereas Figure 2b presents the baseline and monitor perturbations together $\Delta s_1 + \Delta s_2$. (We plot all slowness panels using the same color scale and will henceforth omit the scale bar.) We use a 2D elastic finite-difference modeling code (Weiss and Shragge, 2013) to generate baseline and monitor data sets using the P-wave slowness models shown in Figure 2. We use six equally spaced, horizontal density reflectors to introduce reflectivity.

Figure 3a presents the one-way wave-equation migration baseline image using a $s_0 = 0.5$ s/km migration slowness model. The imaged reflectors are horizontal except near the unaccounted-for baseline perturbation at $x = 1.5$ km. We apply 15 iterations of the ASM-IDT inversion scheme discussed above to generate the Δs_1 estimate shown in Figure 3b. Figure 3c presents the baseline data remigrated with slowness model $s_0 + \Delta s_1$. Note that the baseline slowness estimate is a good approximation of the true perturbation (Figure 2a) and effectively flattens the six reflectors (Figure 3c).

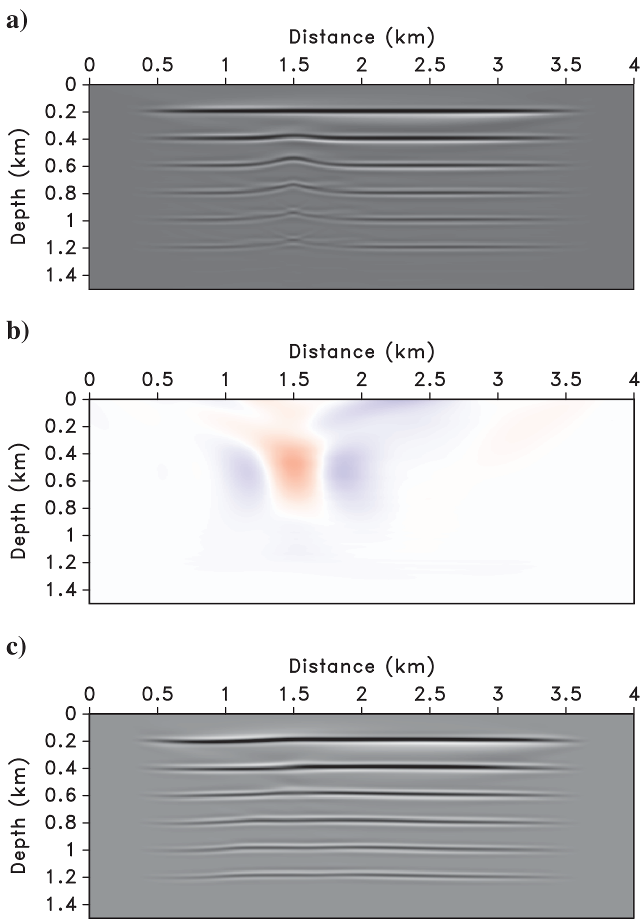

Figure 3. Baseline inversion experiment. (a) Baseline image generated using background model $s_0 = 0.5$ s/km. (b) Inverted baseline perturbation estimate Δs_1. (c) Baseline image using migration slowness $s_0 + \Delta s_1$.

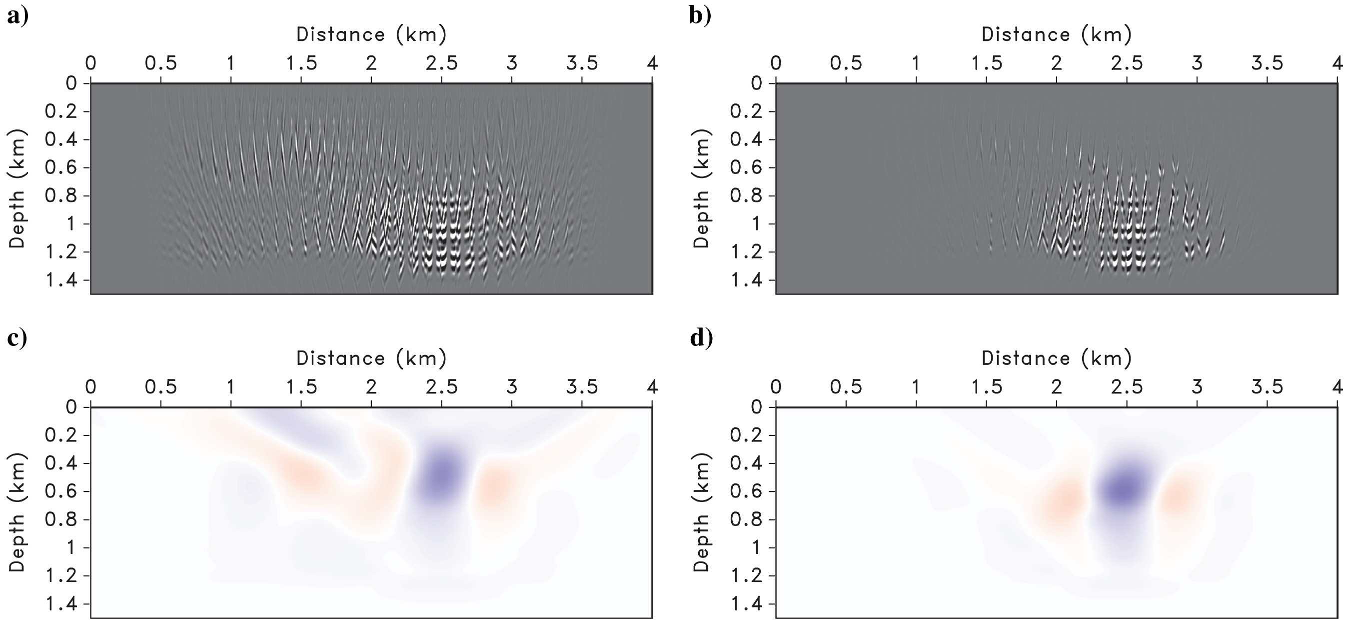

Figure 4. Monitor images and inversion results using slowness profile $s_0 + \Delta s_1$. (a) Horizontal concatenation of P_λ penalized (lagged) correlation gathers. (b) As in (a) but for the P_{4D} penalty operator. (c) Estimated absolute 4D slowness perturbation Δs_2 using P_λ. (d) Estimated relative 4D slowness perturbation Δs_2 using P_{4D}.

We now use the estimated baseline slowness model $s_0 + \Delta s_1$ to migrate the monitor data. Figure 4a and 4b present a horizontal concatenation of the resulting penalized extended image offset gathers (i.e., $\mathcal{H}$ in equation 2 before summation). Figure 4a shows the effect of applying P_λ. We observe that whereas most of the residual energy is located in the vicinity of the monitor slowness perturbation, some unflattened energy remains between $x = 0.5$–2.0 km due to an imperfect baseline velocity analysis as well as aperture/illumination effects. In general, this suggests that using a DSO penalty can lead to contaminated estimates of Δs_{TL}, because residual energy from the baseline analysis can leak into the monitor inversion. Figure 4b presents the monitor image residuals after applying the P_{4D} penalty operator. Here, the consistency in the migrated baseline and monitor images, as encapsulated in the P_{4D} operator, effectively masks the residual energy between $x = 0.5$–2.0 km. The remaining energy is more correctly associated with monitor perturbation Δs_2, and it yields better results than the P_λ-weighted experiment.

Figure 4c and 4d presents the Δs_{TL} estimates from the absolute and relative strategies, respectively, using the inverted baseline result as the initial model. We observe that using the P_{4D} leads to the more restricted image-domain residuals and helps to spatially localize the imaged perturbation. We also note that the absolute ASM-IDT inversion is still incorporating the imperfectly recovered baseline slowness perturbation into the monitor update, which represents “4D inversion leakage” between survey vintages and would introduce erroneous interpretation.

CONCLUSIONS

We have presented an extension of 3D ASM-IDT inversion to 4D scenarios, and we discussed absolute and relative inversion strategies that apply different penalty operators to the imaged wavefield components. Because the relative inversion strategy couples the baseline and monitor data sets by incorporating the baseline image into the monitor penalty operator, this allows consistently, though not necessarily optimally, imaged reflectivity to be removed leading to more robust 4D ASM-IDT inversion results.

ACKNOWLEDGMENTS

We thank D. Lumley for helpful discussions and the reviews of J. Blanch, D.-J. Min, and an anonymous reviewer. J. Shragge acknowledges support of the UWA:RM Consortium sponsors. Simulation results were computed using IVEC HPC facilities. The reproducible numerical examples use the Madagascar package (http://www.ahay.org).

REFERENCES

Albertin, U., 2011, An improved gradient computation for adjoint wave-equation reflection tomography: 81st Annual International Meeting, SEG, Expanded Abstracts, 3969–3973.

Albertin, U., P. Sava, J. Etgen, and M. Maharramov, 2006, Adjoint wave-equation velocity analysis: 76th Annual International Meeting, SEG, Expanded Abstracts, 3345–3349.

Knyazev, A., and I. Lashuk, 2007, Steepest descent and conjugate gradient methods with variable preconditioning: Matrix Analysis and Applications, **29**, 1267–1280, doi: 10.1137/060675290.

Plessix, R.-E., 2006, A review of adjoint state method for computing the gradient of a functional with geophysical applications: Geophysical Journal International, **167**, 495–503, doi: 10.1111/j.1365-246X.2006.02978.x.

Pratt, R. G., 1999, Seismic waveform inversion in the frequency domain, Part 1: Theory and verification in a physical scale model: Geophysics, **64**, 888–901, doi: 10.1190/1.1444597.

Shen, P., W. Symes, S. Morton, and H. Calandra, 2005, Differential semblance velocity analysis via shot profile migration: 75th Annual International Meeting, SEG, Expanded Abstracts, 2249–2252.

Symes, W., 2008, Migration velocity analysis and waveform inversion: Geophysical Prospecting, **56**, 765–790, doi: 10.1111/j.1365-2478.2008.00698.x.

Symes, W. W., and J. J. Carazzone, 1991, Velocity inversion by differential semblance optimization: Geophysics, **56**, 654–663, doi: 10.1190/1.1443082.

Tarantola, A., 1984, Inversion of seismic reflection data in the acoustic approximation: Geophysics, **49**, 1259–1266, doi: 10.1190/1.1441754.

Weiss, R., and J. Shragge, 2013, Solving the 3D anisotropic elastic wave-equation on parallel GPU devices: Geophysics, **78**, no 2, F7–F15, doi: 10.1190/geo2012-0063.1.

Yang, T., and P. Sava, 2011, Image-domain waveform tomography with two-way wave-equation: 81st Annual International Meeting, SEG, Expanded Abstracts, 2591–2596.

Yang, T., J. Shragge, and P. Sava, 2012, Illumination compensation for image-domain wavefield tomography: 74th Annual International Conference and Exhibition, EAGE, Extended Abstracts.